*Supplementary Information*

# Enantioselective Assembly of Tetrahedral $Zr_4$(embonate)$_6$ Cages in Zeolitic Frameworks for Synergetic Circularly Polarized Luminescence

Xin Meng [a,b], Qing-Rong Ding [a], Shu-Mei Chen [b], Yan-Ping He [a,*] and Jian Zhang [a,*]

[a] State Key Laboratory of Structural Chemistry, Fujian Institute of Research on the Structure of Matter, Chinese Academy of Sciences, Fuzhou, Fujian 350002, P. R. China.

[b] College of Chemistry, Fuzhou University, Fuzhou, Fujian 350108, China.

* Corresponding Author: hyp041@163.com; zhj@fjirsm.ac.cn.

## 1. Experimental section.

**Materials and instrumentation:** Reagents were purchased commercially and used without further purification. Embonic acid ($H_4L$) and chiral (R)-(+)-2,2'-bis(diphenylphosphino)-1,1'-binaphthyl/(S)-(-)-2,2'-bis(diphenylphosphino)-1,1'-binaphthyl (R/S-BINAP) ligands were purchased commercially. All syntheses were carried out in a 20 mL vial under autogenous pressure. Thermogravimetric (TGA) analysis was performed on a Netzch STA449F3 analyzer at a heating rate of 10 ℃/min from ambient temperature to 800 ℃ under $N_2$ atmosphere. Powder XRD was recorded on a Rigaku Dmax/2500 diffractometer with Cu Kα radiation (λ=1.54056 Å) with a step size of 0.05°. UV−vis absorption spectra were measured on a PerkinElmer Lambda 950 UV−vis spectrophotometer. Fluorescence spectra were measured with a HORIBA Jobin-Yvon FluoroMax-4 spectrometer. The solid-state circular dichroism (CD) spectra were measured on an MOS-450 spectropolarimeter. The PL spectra were finished on the UV/V/NIR Fluorescence Spectrometer (Edinburgh, FLS1000) and Circularly Polarized Luminescence (CPL-300).

**Synthesis of $(Me_2NH_2)_8[(Zr_4L_6)]$·Guests (PTC-101(Δ,Λ)).** PTC-101(Δ,Λ) as the staring raw material of $Zr_4L_6$ cages can be synthesized in large quantities by the method reported in our previous work.[1,2] $H_4L$ (8 g, 20 mmol), $Zr(OnPr)_4$ (5 mL, 14 mmol) and en (4 mL, en=ethylenediamine) were added to 240 mL n-propanol/DMF (2:1, v/v, DMF=N,N-dimethylformamide) solvents and mixed at room temperature. The resultant solution was sealed in a 500 mL reaction bottle and heated at 100 ℃ for 5 days. After cooled to room temperature, ~ 7 g yellow crystals of PTC-101(Δ,Λ) were obtained. Its synthetic route and crystal structure are shown in Figure S1.

**Synthesis of $(Me_2NH_2)_9[(\Delta\Delta\Delta\text{-}Zr_4L_6)]Cl$·Guests (PTC-102(Δ)) and $(Me_2NH_2)_9[(\Lambda\Lambda\Lambda\text{-}Zr_4L_6)]Cl$·Guests (PTC-102(Λ)).** PTC-102(Δ) and PTC-102(Λ) can also be used as the staring raw material of $Zr_4L_6$ cages, but which was synthesized in low yield.[1] $H_4L$ (120 mg, 0.3 mmol), $ZrCl_4$ (90 mg, 0.4 mmol) and 2 drops of en were added to 6 mL of n-propanol/DMF (3:1, v/v) and mixed at room temperature. The resultant solution was heated at 100 ℃ for two days. After cooled to room temperature, ~ 20 mg yellow crystals of PTC-102(Δ) and PTC-102(Λ) were obtained in the same reaction bottle. Its synthetic route and crystal structure are shown in Figure S2.

**X-ray Crystallography.** Crystallographic data for **PTC-374(R,Δ)**, **PTC-374(S,Λ)**, **R-Ag** and **S-Ag** were collected on a Supernova single-crystal diffractometer equipped with

graphite-monochromatized Mo or Cu Kα radiation (λ=0.71073 Å or 1.54184 Å) at 293 or 297 K. Absorption correction was applied using SADABS.[3] The structure was solved by direct method and refined by full-matrix least-squares on F2 using SHELXTL.[4] In these structures, some free solvent molecules were highly disordered and could not be located. The diffused electron densities resulting from these residual solvent molecules were removed from the data set using the SQUEEZE routine of PLATON[5] and refined further using the data generated. Crystal data and details of data collection and refinement of **PTC-374(R,Δ)**, **PTC-374(S,Λ)**, **R-Ag** and **S-Ag** are summarized in Tables S1 and S2. CCDC 2356638-2356641 contain the supplementary crystallographic data for this paper. These data are provided free of charge by The Cambridge Crystallographic Data Centre.

**References：**


[1] Y.-P. He, L.-B. Yuan, G.-H. Chen, Q.-P. Lin, F. Wang, L. Zhang, J. Zhang, Water-Soluble and Ultrastable $Ti_4L_6$ Tetrahedron with Coordination Assembly Function, *J. Am. Chem. Soc.*, 2017, **139**, 16845-16851.

[2] Y.-F. Li, Y.-P. He, Q.-H. Li, J. Zhang, Integrated Anionic Zirconium-Organic Cage and Cationic Boron-Imidazolate Cage for Synergetic Optical Limiting, *Angew. Chem. Int. Ed.*, 2024, **63**, e202318806.

[3] G. M. Sheldrick, SADABS, Program for area detector adsorption correction. *Institute for Inorganic Chemistry*, University of Göttingen, Göttingen (Germany), 1996.

[4] G. M. Sheldrick, SHELXL-2014/7: *A Program for Structure Refinement*, University of Göttingen, Göttingen, Germany, 2014.

[5] P. van der Sluis, A. L. Spek, *Acta Cryst. A.* 1990, **46**, 194–201.

**Table S1.** Crystallographic Data and Structure Refinement Details for Compounds **PTC-374(R,Λ)** and **PTC-374(S,Λ)**.

| **Compound** | **PTC-374(R,Λ)** | **PTC-374(S,Λ)** |
|---|---|---|
| CCDC | 2356638 | 2356639 |
| formula | $C_{278}H_{180}N_4O_{36}P_6Ag_{2.5}Zr_4$ | $C_{280}H_{180}N_4O_{36}P_6Ag_{2.5}Zr_4$ |
| formula weight | 4972.62 | 4996.64 |
| crystal system | cubic | cubic |
| space group | *I*23 | *I*23 |
| *a* (Å) | 38.8066(3) | 38.8309(4) |
| *b* (Å) | 38.8066(3) | 38.8309(4) |
| *c* (Å) | 38.8066(3) | 38.8309(4) |
| *α* (°) | 90 | 90 |
| *β* (°) | 90 | 90 |
| *γ* (°) | 90 | 90 |
| *V* (Å$^3$) | 58440.9(14) | 58550.7(18) |
| *Z* | 8 | 8 |
| $D_{calcd}$ (g·cm$^{-3}$) | 1.130 | 1.134 |
| *μ*(Cu K*a*) (mm$^{-1}$) | 3.241 | 3.237 |
| *F*(000) | 20252 | 20348 |
| temperature (K) | 293(2) | 293(2) |
| theta min, max (deg) | 2.277, 54.227 | 2.276, 75.971 |
| tot., uniq. Data | 47036/47036 | 49550/17249 |
| *R* (int) | 0.0571 | 0.0699 |
| observed data[($I > 2\sigma(I)$] | 26378 | 8339 |
| $N_{ref}$, $N_{par}$ | 47036, 850 | 17249, 856 |
| $R_1$, $wR_2$ (all data)[a] | 0.0800, 0.2552 | 0.1088, 0.3706 |
| *S* | 1.050 | 1.135 |
| Min and max resd dens (e·Å$^{-3}$) | -0.38, 0.56 | -0.64, 0.44 |
| Flack parameter | 0.016(7) | 0.035(8) |

**Table S2.** Crystallographic Data and Structure Refinement Details for **R-Ag** and **S-Ag**.

| **Compound** | **R-Ag** | **S-Ag** |
|---|---|---|
| CCDC | 2356640 | 2356641 |
| formula | $C_{88}H_{64}O_4P_4ClAg$ | $C_{88}H_{64}O_4ClP_4Ag$ |
| formula weight | 1452.59 | 1452.59 |
| crystal system | orthorhombic | orthorhombic |
| space group | $P2_12_12_1$ | $P2_12_12_1$ |
| *a* (Å) | 12.02620(10) | 12.0113(2) |
| *b* (Å) | 21.6512(3) | 21.6324(4) |
| *c* (Å) | 28.7849(3) | 28.7482(5) |
| $\alpha$ (°) | 90 | 90 |
| $\beta$ (°) | 90 | 90 |
| $\gamma$ (°) | 90 | 90 |
| *V* (Å$^3$) | 7495.06(14) | 7469.7(2) |
| *Z* | 4 | 4 |
| $D_{calcd}$ (g·cm$^{-3}$) | 1.287 | 1.293 |
| $\mu$(Mo/Cu K$\alpha$) (mm$^{-1}$) | 3.689 | 0.442 |
| *F*(000) | 2992 | 2996 |
| temperature (K) | 293(2) | 297.60(10) |
| theta min, max (deg) | 2.554, 75.558 | 1.701, 30.915 |
| tot., uniq. Data | 39103/13924 | 87469/19671 |
| *R* (int) | 0.0424 | 0.0427 |
| observed data[($I > 2\sigma(I)$] | 12398 | 15678 |
| $N_{ref}$, $N_{par}$ | 13924, 868 | 19671, 858 |
| $R_1$, $wR_2$ (all data)[a] | 0.0520, 0.1706 | 0.0520, 0.1582 |
| *S* | 1.135 | 1.035 |
| Min and max resd dens (e·Å$^{-3}$) | -0.72, 0.97 | -0.85, 0.64 |
| Flack parameter | -0.024(4) | -0.018(7) |

## 2. Simplified synthesis route.

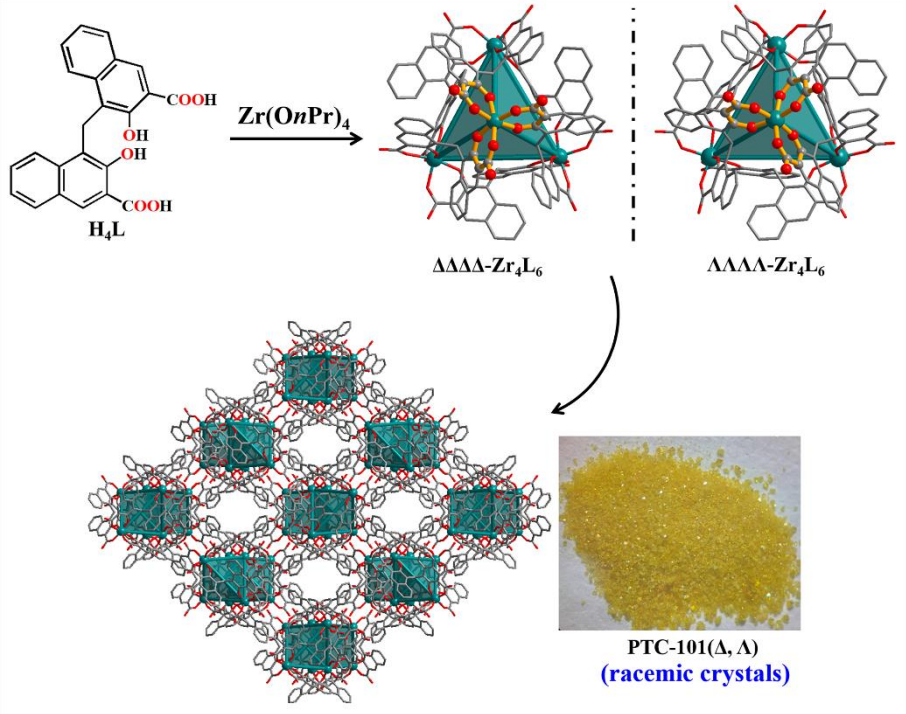


**Figure S1.** The synthetic route of PTC-101(Δ,Λ) and the crystal structure. H atoms have been removed for clarity. Atom color code: olive, Zr; red, O; gray, C.

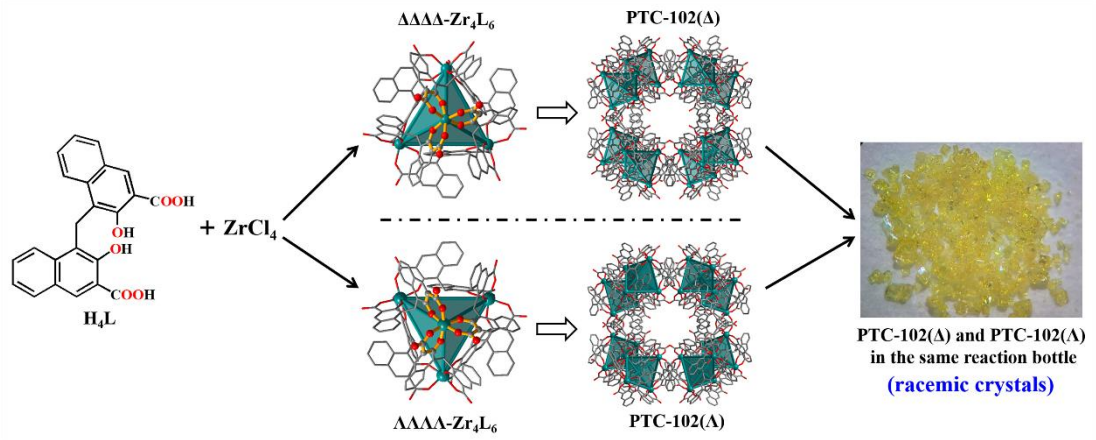


**Figure S2.** The synthetic route of PTC-102(Δ) and PTC-102(Λ) and the crystal structure.

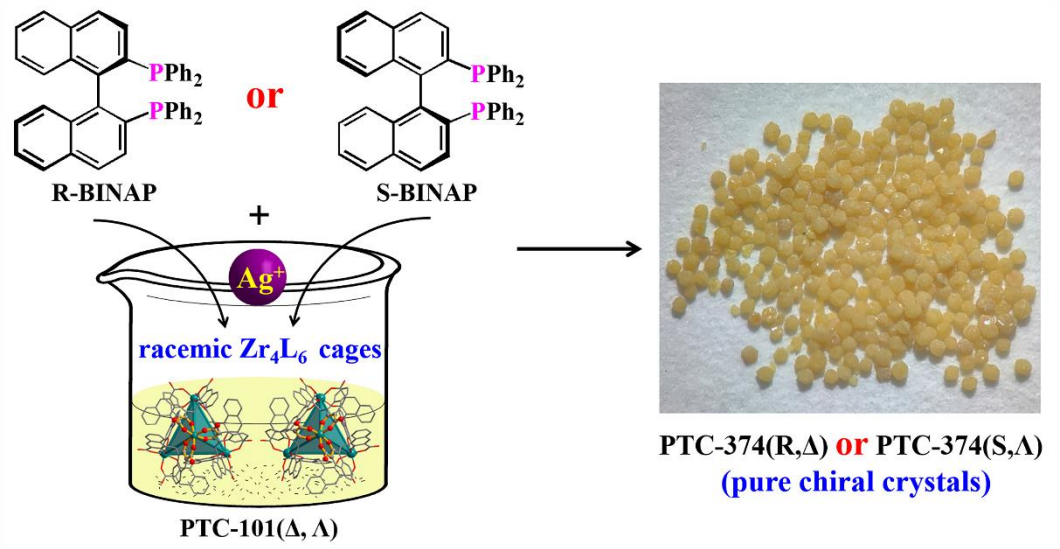


**Figure S3.** The synthetic route of **PTC-374(R,Δ)** and **PTC-374(S,Λ)**.

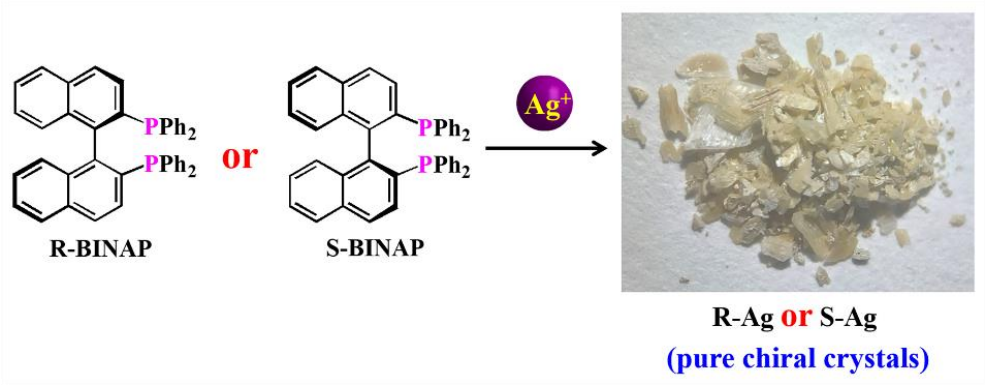


**Figure S4.** The synthetic route of **R-Ag** and **S-Ag**.

## 3. Detailed structural information.

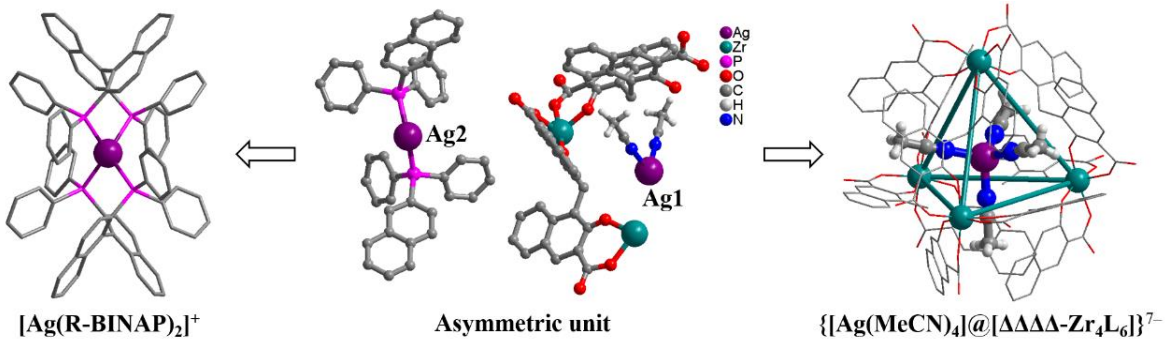


**Figure S5.** (Middle) The asymmetric unit of **PTC-374(R,Δ)**, showing one third of ΔΔΔΔ-$Zr_4L_6$ cage, one third of $[Ag(MeCN)_4]^+$ cation and half of $[Ag(R\text{-}BINAP)_2]^+$ cation (Solvents and $(Me_2NH_2)^+$ countercations could not be located because of highly disorder). (Left) The $[Ag(R\text{-}BINAP)_2]^+$ cation. (Right) The ΔΔΔΔ-$Zr_4L_6$ cage, in which one $[Ag(MeCN)_4]^+$ cation is located in the center of the cage. Most H atoms have been removed for clarity. Atom color code: purple, Ag; olive, Zr; pink, P; red, O; gray, C; off white, H.

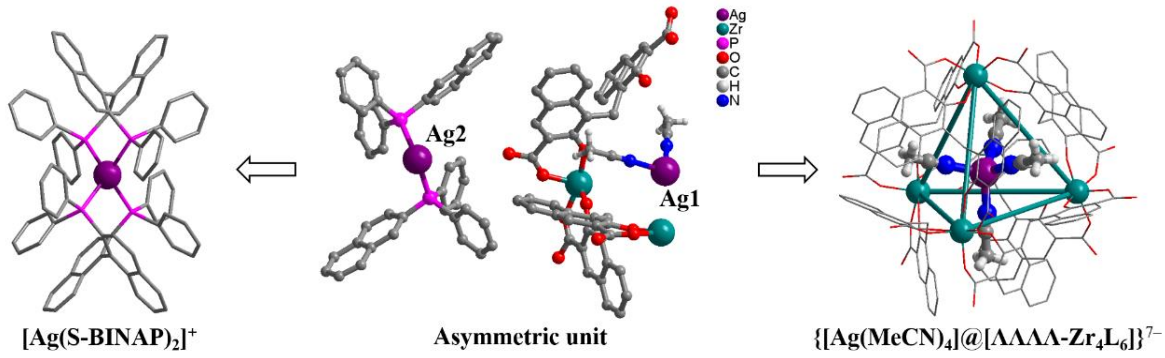


**Figure S6.** (Middle) The asymmetric unit of **PTC-374(S,Λ)**, showing one third of ΛΛΛΛ-$Zr_4L_6$ cage, one third of $[Ag(MeCN)_4]^+$ cation and half of $[Ag(S\text{-}BINAP)_2]^+$ cation (Solvents and $(Me_2NH_2)^+$ countercations could not be located because of highly disorder). (Left) The $[Ag(S\text{-}BINAP)_2]^+$ cation. (Right) The ΛΛΛΛ-$Zr_4L_6$ cage, in which one $[Ag(MeCN)_4]^+$ cation is located in the center of the cage.

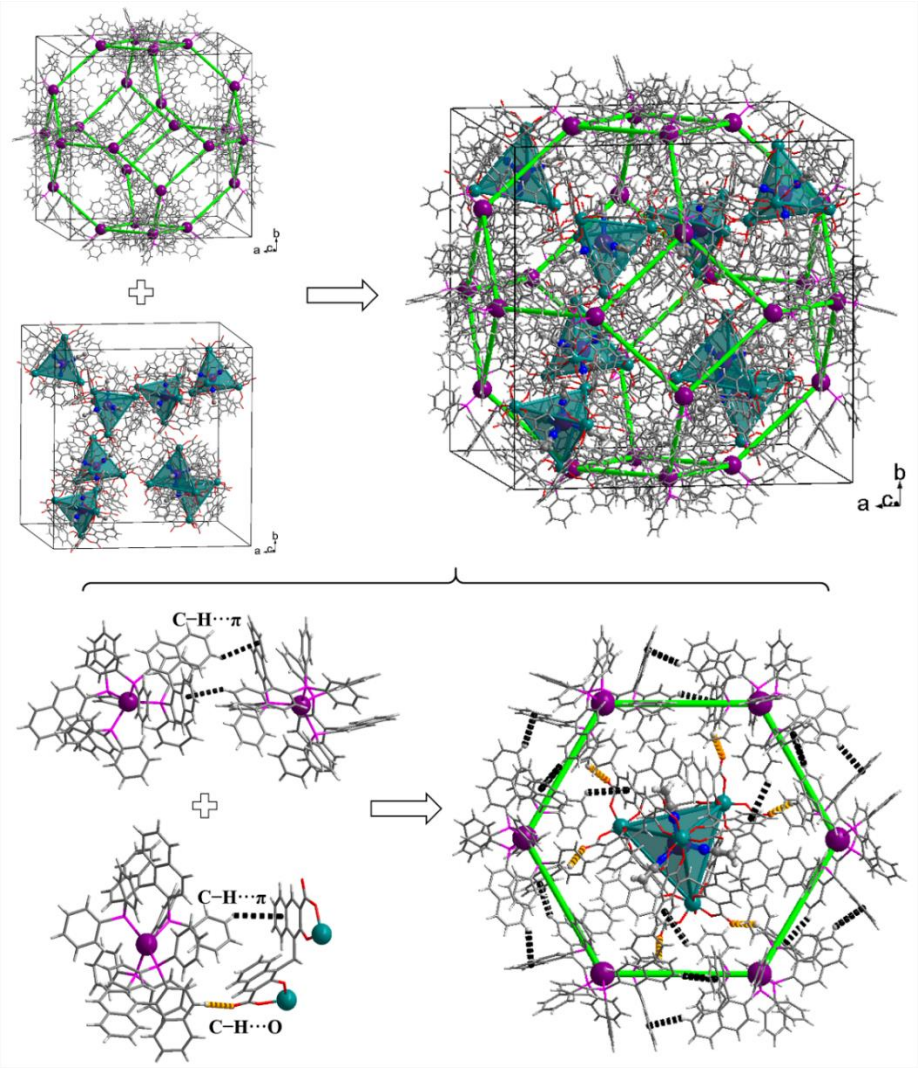


**Figure S7.** Illustration the intergration of $[Ag(MeCN)_4]$@ΛΛΛΛ-$Zr_4L_6$ cages and $[Ag(S\text{-}BINAP)_2]^+$ cations into a 3D supramolecular architecture by the weak interactions in **PTC-374(S,Λ)**.

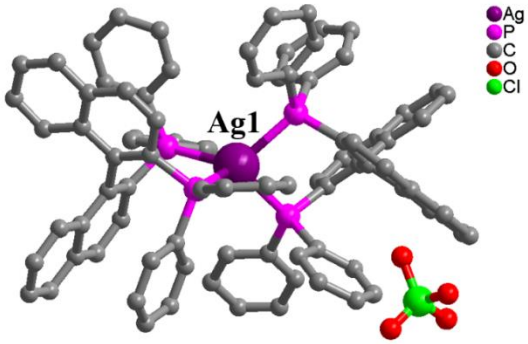


**Figure S8.** The asymmetric unit of **R-Ag**, showing one $[Ag(R\text{-}BINAP)_2]^+$ cation and one $[ClO_4]^-$ counter anion (Solvents could not be located because of highly disorder). H atoms have been removed for clarity. Atom color code: purple, Ag; pink, P; green, Cl; red, O; gray,

C.

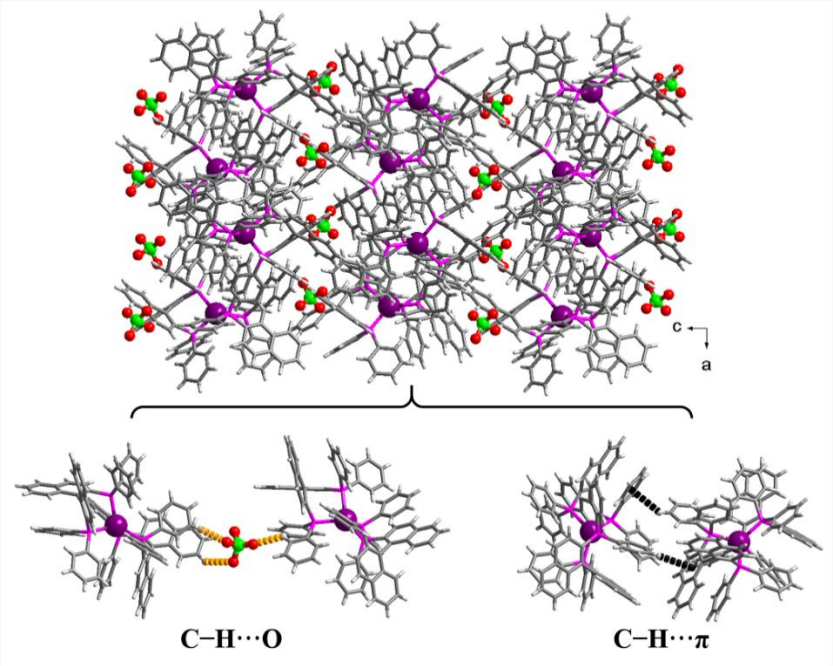


**Figure S9.** The packed structure along the b-axis in **R-Ag**, in which the $[ClO_4]^-$ counter anions are located in the supramolecular structure (top). The supramolecular interactions (bottom).

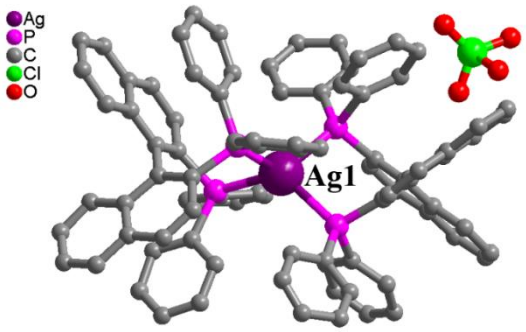


**Figure S10.** The asymmetric unit of **S-Ag**, showing one $[Ag(S\text{-}BINAP)_2]^+$ cation and one $[ClO_4]^-$ counter anion

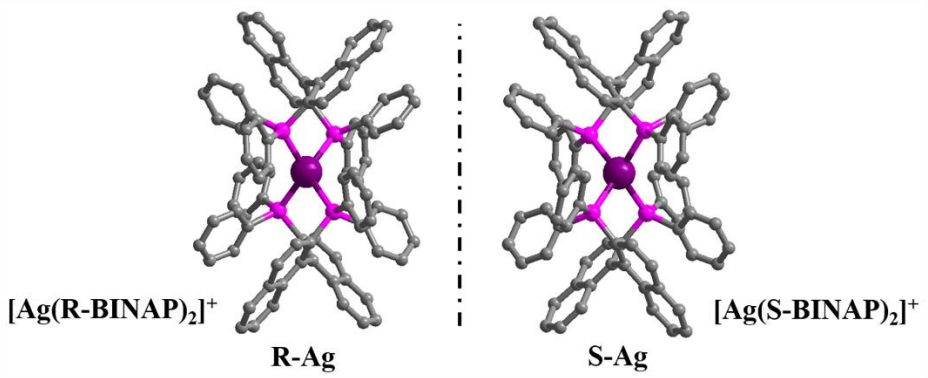


**Figure S11.** The mirror images can be observed in **R-Ag** and **S-Ag**.

## 4.EDS, TG, PXRD data.

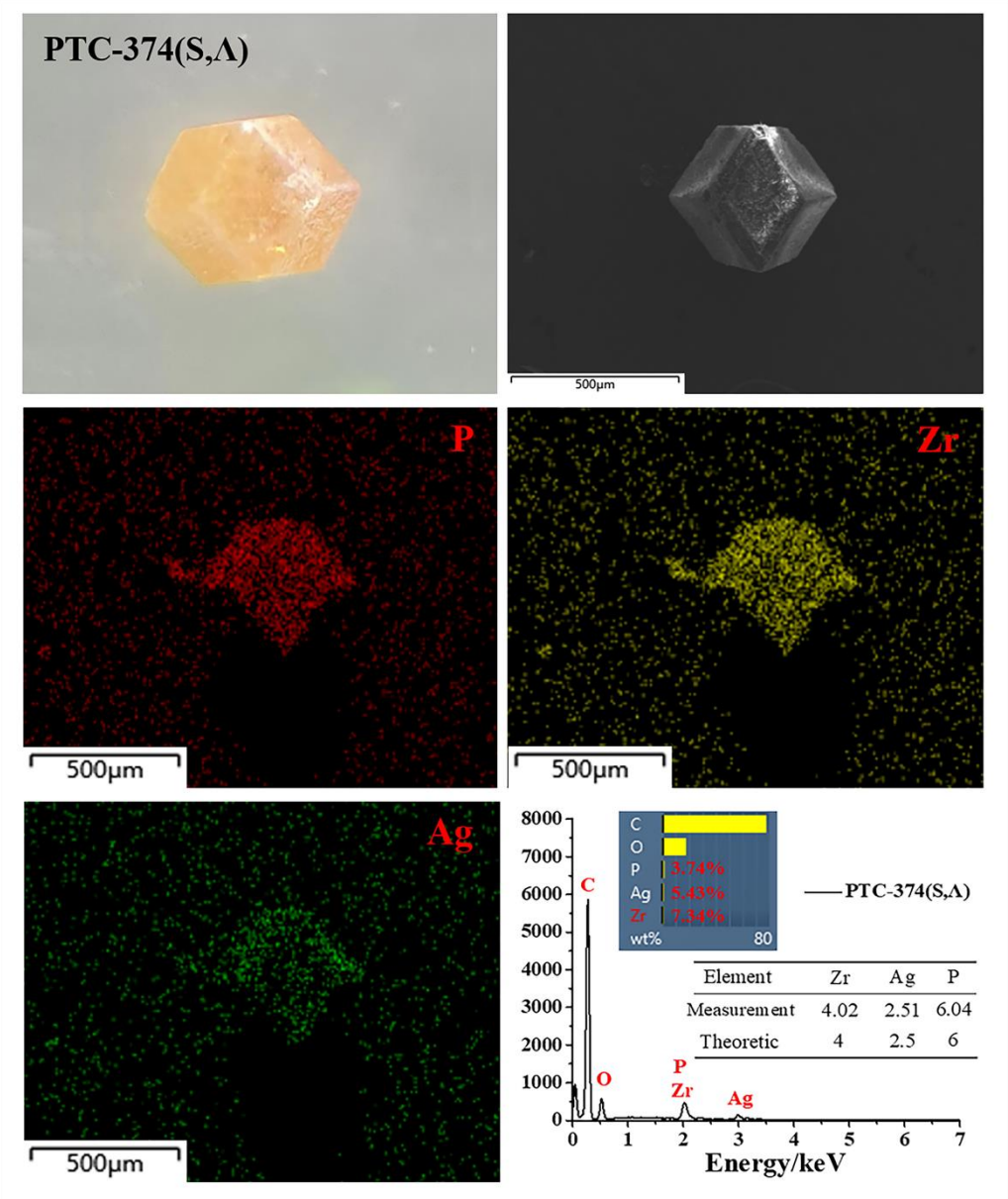


**Figure S12.** Crystal photo of **PTC-374(S,Λ)** and SEM images together with element mappings, and EDS spectrum.

From the EDS data of **PTC-374(S,Λ)**, the elements (mainly Zr, Ag and P) are also analyzed in detail. By calculation, the mass percentage (Wt %) of these elements is converted to the atomic ratio, as shown in Figure S12. The result shows that the atomic ratio of Zr, Ag and P elements is almost consistent with the theoretical (obtained from single crystal structure data), which further indicates the high purity of the sample.

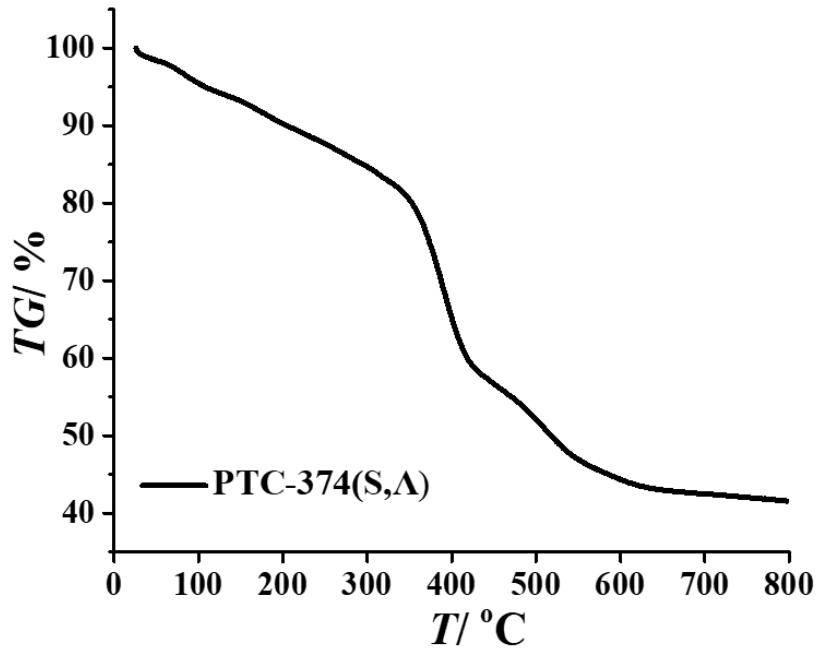


**Figure S13.** TGA curve of **PTC-374(S,Λ)**.

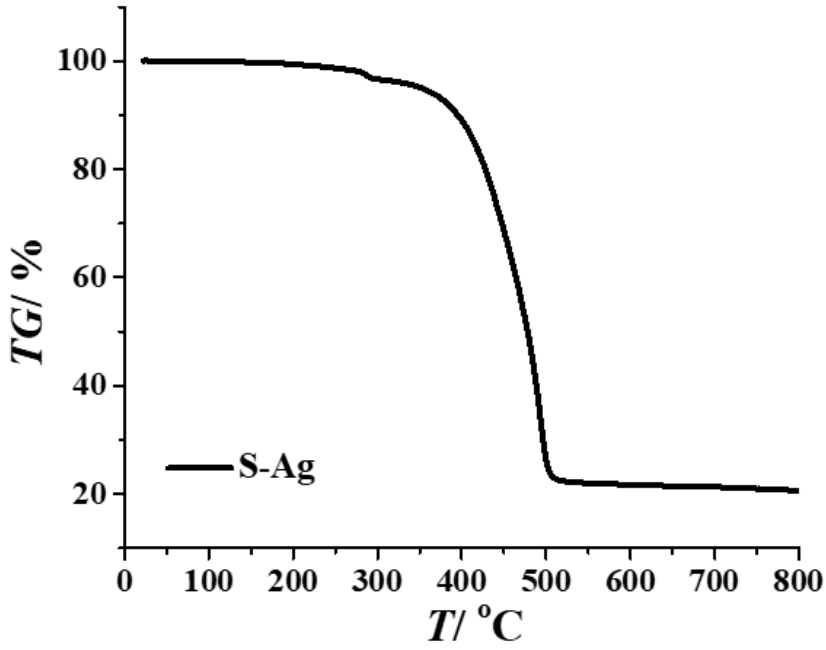


**Figure S14.** TGA curve of **S-Ag**.

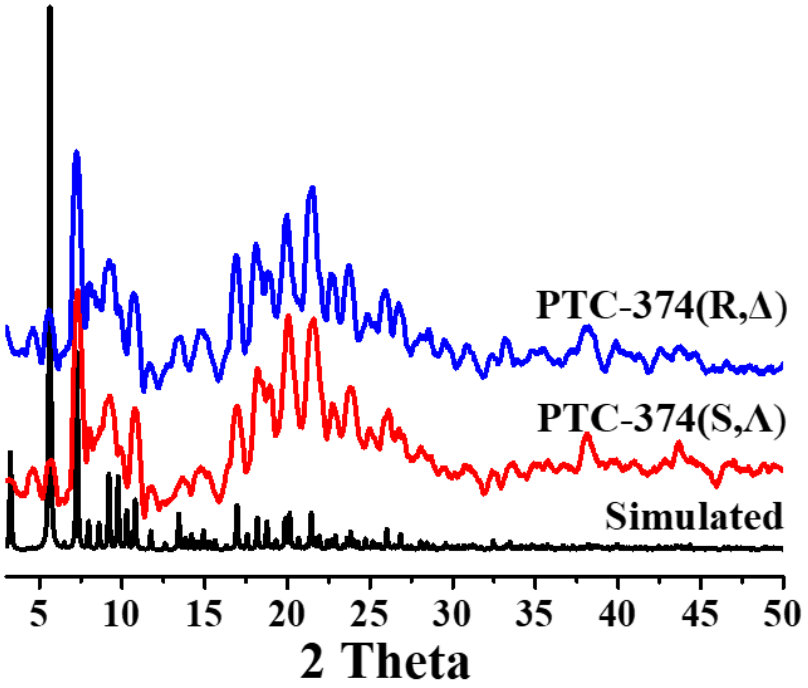


**Figure S15.** PXRD patterns of simulated from the single-crystal data of **PTC-374(S,Λ)** (black) and as-synthesized **PTC-374(S,Λ)** (red) and **PTC-374(R,Δ)** (blue).

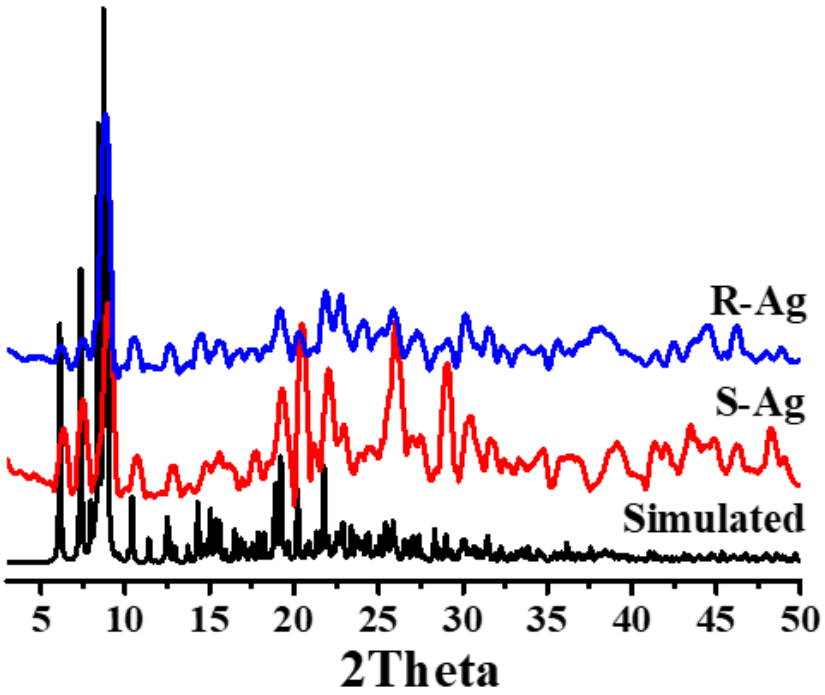


**Figure S16.** PXRD patterns of simulated from the single-crystal data of **S-Ag** (black) and as-synthesized **S-Ag** (red) and **R-Ag** (blue).

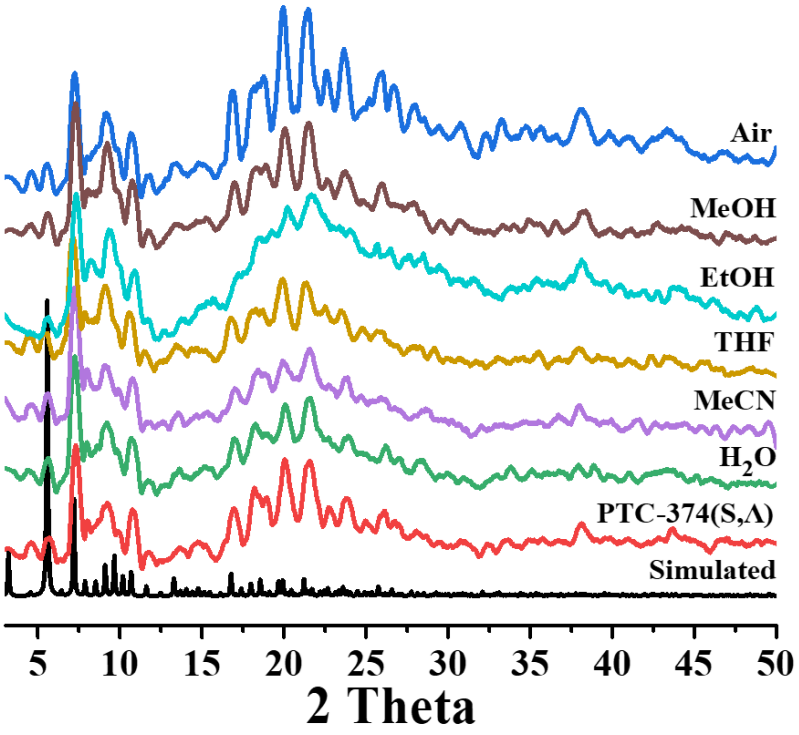


**Figure S17.** PXRD patterns of simulated from the single-crystal data of **PTC-374(S,Λ)** (black), as-synthesized **PTC-374(S,Λ)** (red), and dried crystals of **PTC-374(S,Λ)** immersed in different solvents for 1 day as well as exposed in air for 1 week.

## 5.CD and UV spectra.

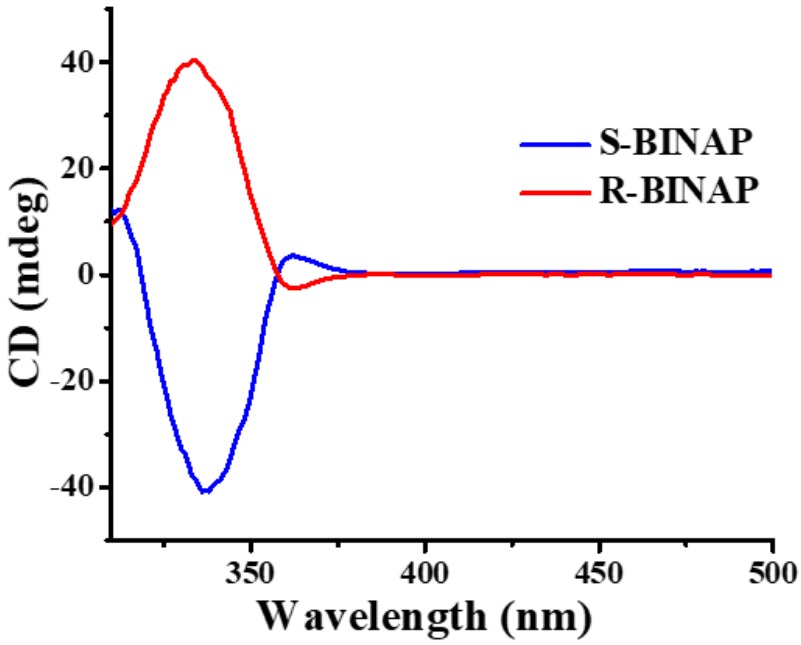


**Figure S18.** Liquid-state CD spectra of R-BINAP and S-BINAP in DMF.

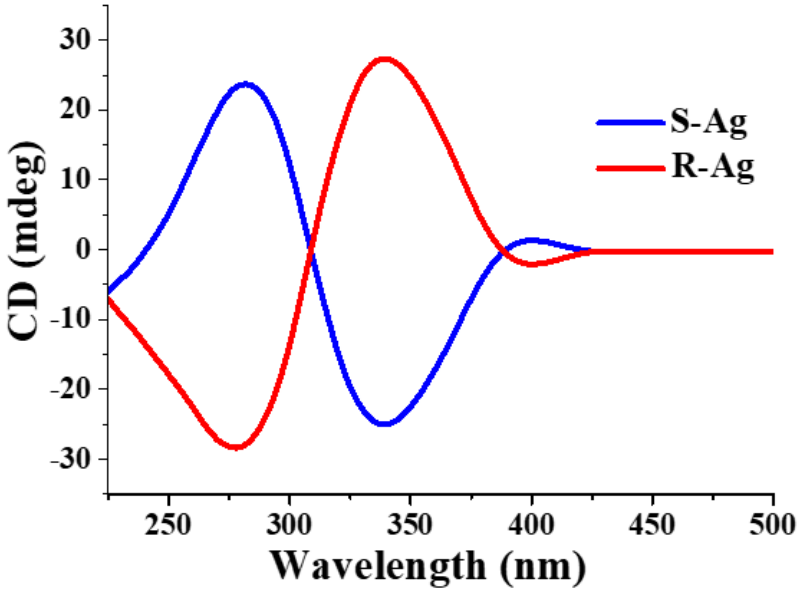


**Figure S19.** Liquid-state CD spectra of **R-Ag** and **S-Ag** in DMF.

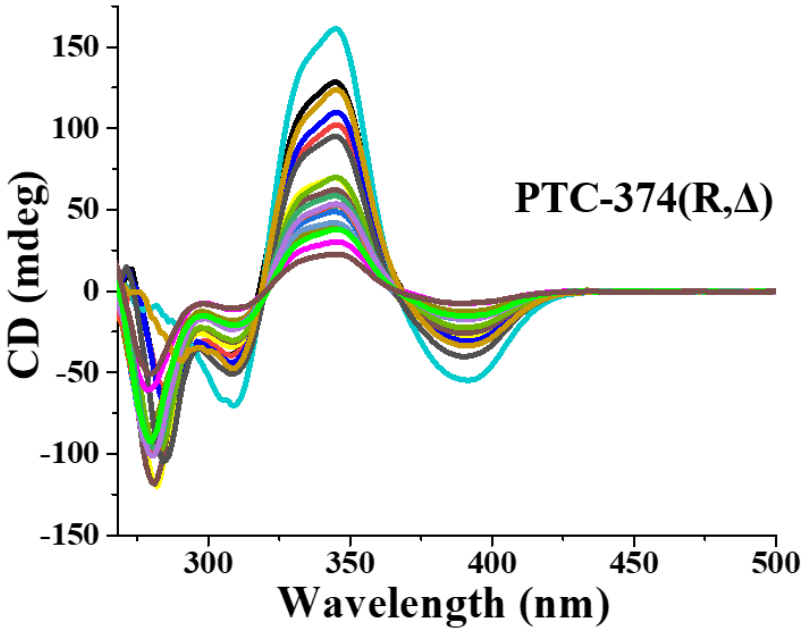


**Figure S20.** Liquid-state CD spectra of different single-crystal of **PTC-374(R,Δ)** in DMF.

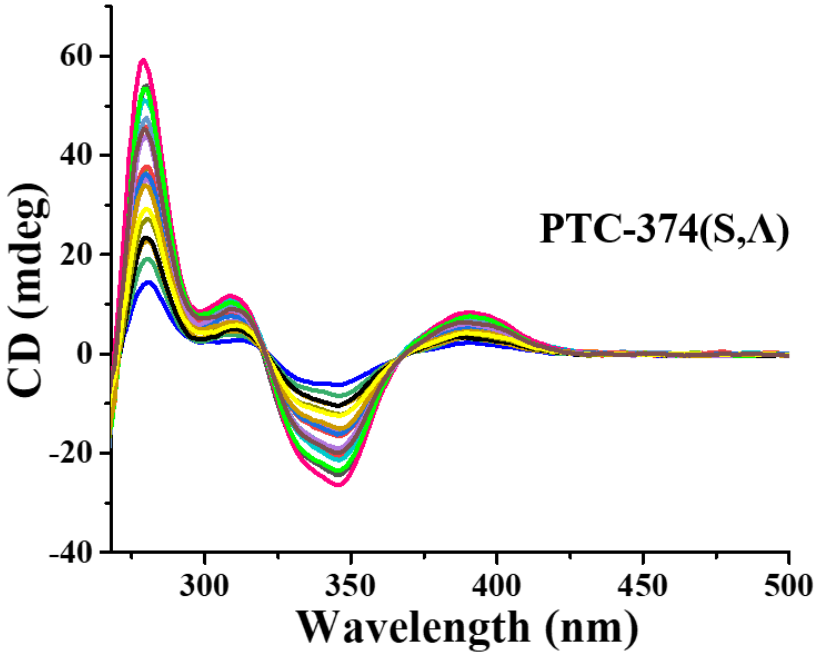


**Figure S21.** Liquid-state CD spectra of different single-crystal of **PTC-374(S,Λ)** in DMF.

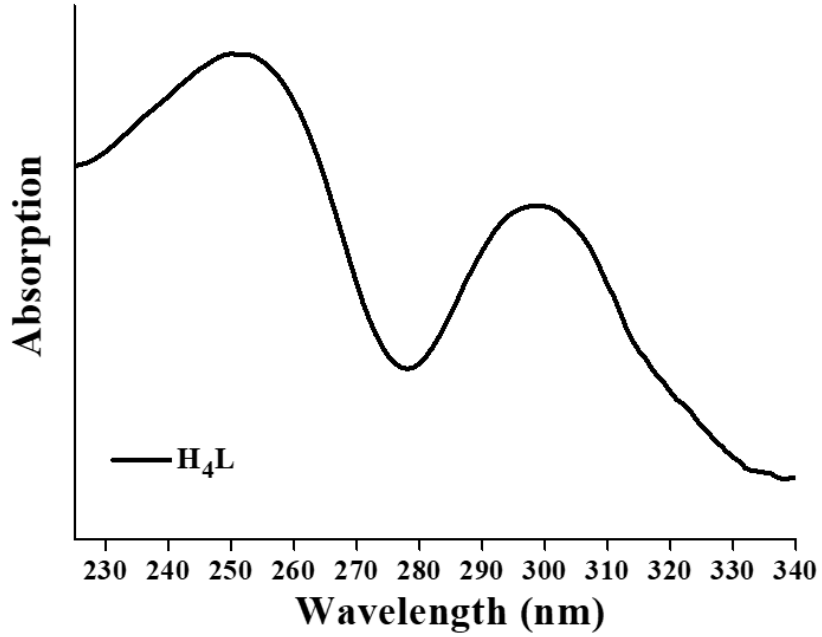


**Figure S22.** Solid-state UV absorption spectrum of the $H_4L$ ligand.

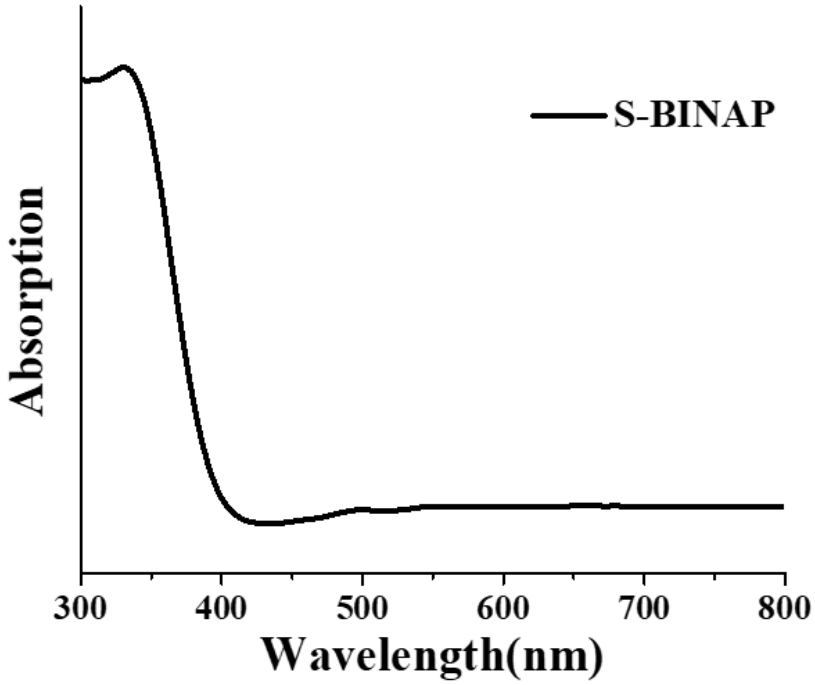


**Figure S23.** Solid-state UV absorption spectrum of the S-BINAP ligand.

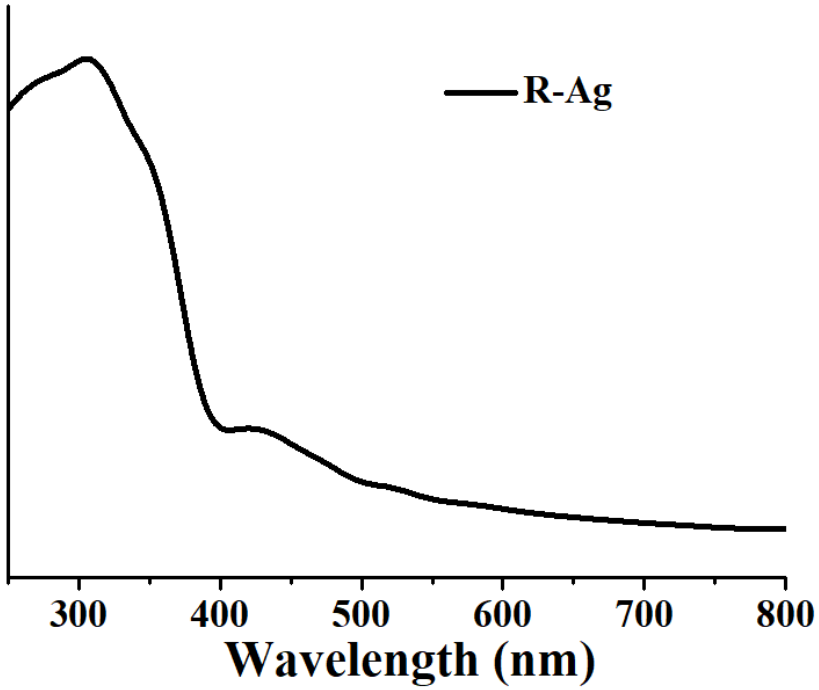


**Figure S24.** Solid-state UV absorption spectrum of **R-Ag**.

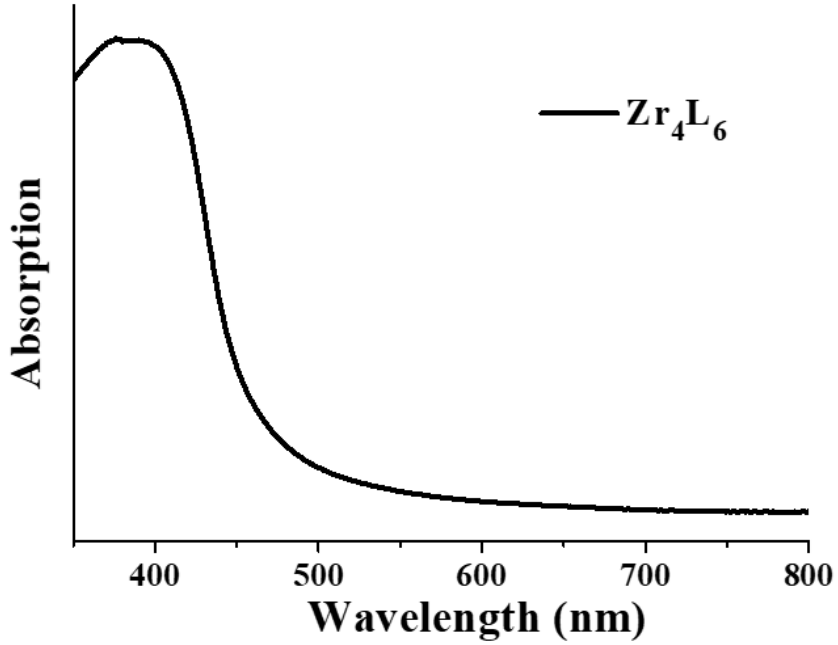


**Figure S25.** Solid-state UV absorption spectrum of $Zr_4L_6$ cage (PTC-102(Δ) and PTC-102(Λ)).

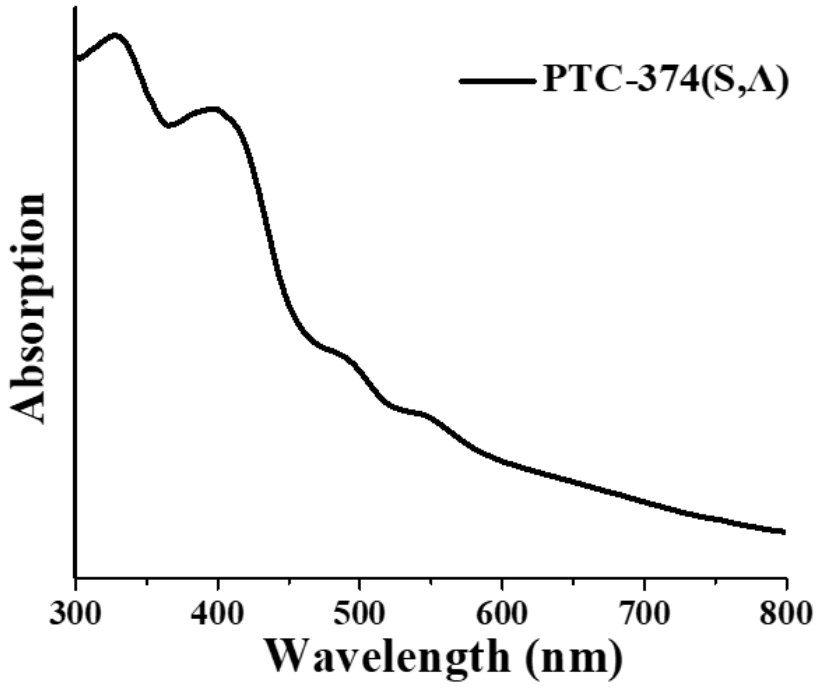


**Figure S26.** Solid-state UV absorption spectrum of **PTC-374(S,Λ)**.

## 6. Optical property study.

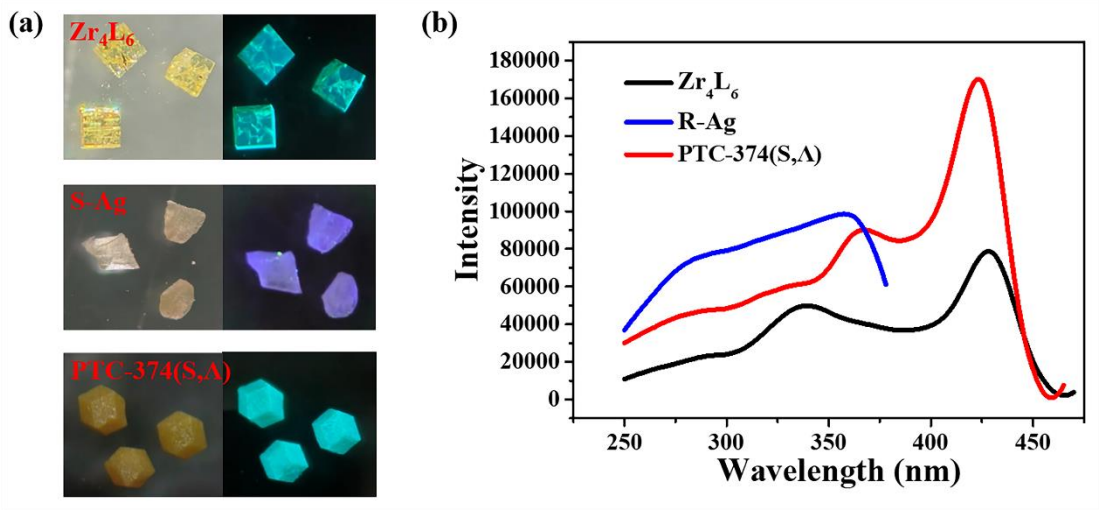


**Figure S27.** (a) The crystal photos of $Zr_4L_6$ cage (PTC-102(Δ) and PTC-102(Λ)), and **PTC-374(S,Λ)**, and their photos before and after ultraviolet light (365 nm). (b) The excitation spectra measured in air at room temperature.

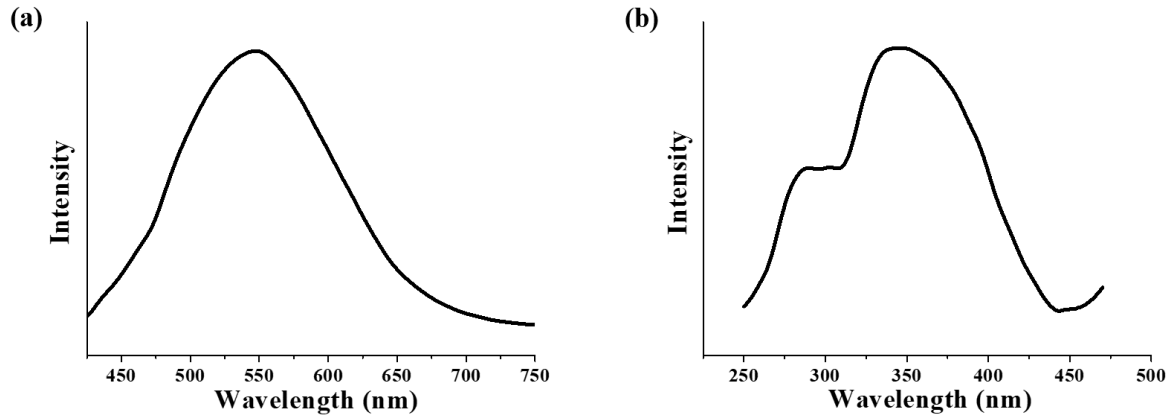


**Figure S28.** The emission (a) and excitation (b) spectra of free L ligand measured in air at room temperature.

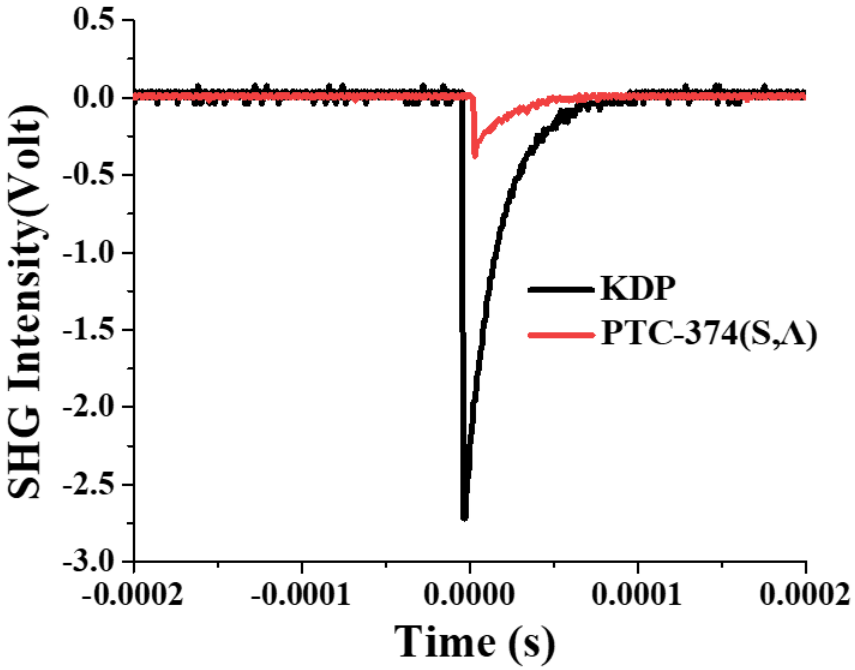


**Figure S29.** Comparison of the measured SHG response of **PTC-374(S,Λ)** with that of KDP at the same particle size of 125−180 μm.

Since **PTC-374(S,Λ)** crystallizes in chiral space group, its second-harmonic generation (SHG) property was studied by using an Nd:YAG laser (1064 nm) (Figure S29). The SHG measurement was carried out on the microcrystalline sample, using 1064 nm radiation, and the result reveals that the bulk material for **PTC-374(S,Λ)** displays weak powder SHG efficiency, which is approximately 0.13 times that of a potassium dihydrogen phosphate (KDP) powder in the particle size of 125−180 μm.